An Analytical Approach for Describing the Bond Mechanism Between FRP and Curved Masonry Substrate

Yu Yuan and Gabriele Milani(✉)

Department of Architecture, Built Environment and Construction Engineering (ABC), Politecnico di Milano, Piazza Leonardo da Vinci 32, 20133 Milan, Italy
gabriele.milani@polimi.it

Abstract. Nowadays, the application of externally bonded FRP (Fiber Reinforced Polymer) material to reinforcement projects for existing buildings has become quite usual. In the applications of masonry structures, the curved masonry members, including arches, vaults, domes, etc., as common bearing components in masonry structures, have also received attention. The curvature of the substrate will introduce additional normal stress to the FRP-masonry interface, leading to different bond behaviors according to experimental observations. This paper attempts to reproduce the behavior of FRP strengthened curved masonry prism under shear, under the assumption of a classical model including three parts of an elastic FRP strip, a zero-thickness interface, and a rigid substrate. By simplifying the interface stress-slip law into a three-stage linear relationship, i.e., the initial elastic stage, the softening stage, and the residual strength stage, the analytical solutions of the stress and strain along the full length of the FRP can be obtained. The effect of the normal stress appearing along the interface is manifested by the change in the interface relationship. The effectiveness of the analytical model is verified by comparison with existing experimental data and numerical model. Due to the fast and stable calculation procedure, this model can explore the influence of various parameters on the model behavior at a small computational cost, and give some insight into the bonding mechanism of FRP reinforced curved structures.

Keywords: FRP strengthening · Masonry · Closed-form solution · Bond-slip model

1 Introduction

In recent years, the strengthening approach of externally applying FRP (Fiber Reinforced Polymer) onto structure surface has been proved to be efficient and holds several advantages such as fast and flexibility, small space occupation, and little effect on structure self-weight. This composite material has also been widely applied in masonry structures when the issues regarding material compatibility are not serious, and the reversibility controversy regarding architectural heritages doesn't exist. There have been many practical engineering cases and related research [1, 2]. One topic received less attention yet

R. Capozucca et al. (Eds.): ICSCES 2022, LNCE 317, pp. 199–209, 2023.
https://doi.org/10.1007/978-3-031-24041-6_16

quite common is that, the reinforcement of curved structures such as arches, vaults, and domes, which are important and common load-bearing members. When adopting an externally bonded approach for such structures, the curvature of the substrate will bring additional normal stress along the FRP-masonry interface, and it can be predicted that the effect of bonding will be affected to a certain extent.

At present, an experimental approach to test the bond behavior of FRP strengthened curved masonry structures on the basis of the classic shear test was developed [3, 4], meanwhile loading tests directly on reinforced arches or vaults were carried out as well [5–7]. Furthermore, some predictive models were developed, either based on the analysis model [8, 9] or using numerical modeling methods [10–12]. The single-lap shear tests conducted by Rotunno et al. [3] can be unutilized as a starting point for modeling assumptions, and an approach to verify the current research. In this experimental campaign, a modified experimental set-up (see Fig. 1) was developed to test the bond behavior of five sets of carbon-FRP reinforced curved masonry prisms. Both internal and external strengthening approaches were considered, and each approach was tested with one higher and one lower substrate curvature, as well as flat prisms, were tested for comparison. Cohesive failure (CF), interface failure (IF), prismatic failure (PF), and fiber failure (FF) were observed during the testing. For most intrados cases, the combination of CF (near the loading edge) and IF (near the free edge) modes occurred, it can be explained that, the peeling effect brought by the substrate curvature became prominent after part of the FRP strip was detached. While for extrados cases, the most common failure mode is CF.

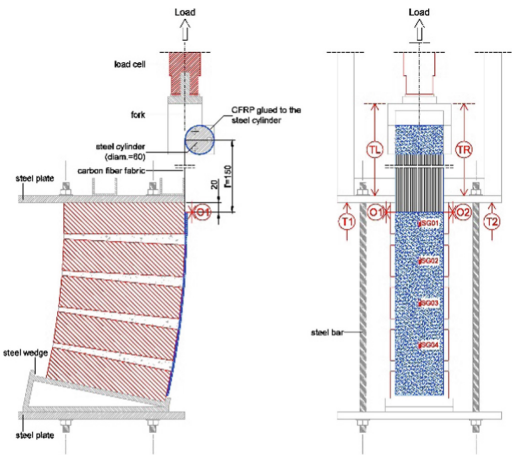

Fig. 1. The shear test set-ups for strengthened curved masonry prisms [3]

These experimental facts give us the opportunity to consider an FRP strip with elastic behavior, a rigid substrate in our model, and an interface that lumped all the non-linearities being the only position where the failure can occur. Furthermore, the experimental results also reveal that the load-bearing capacity is promoted for the extrados strengthening case, while deduced for the intrados case compared to the flat one.

And the load-bearing capacity for extrados (intrados) cases increases (decreases) with the curvature, indicating that the curvature of the substrate plays an important role in the curved cases. After we lumped all the non-linearities along the interface, the influence of curvature can be taken into account in the interfacial relationship by the effect of normal stress on friction.

In this article, an analytical model to reproduce the bond behavior under the first experimental approach will be introduced. Compared to some existing modeling approaches, this approach only asks for a few simple and clearly-defined parameters while can quickly and steadily produce results of both global and local bond behavior, which allows for exploration of the theoretical bond mechanism with little computational effort. The article is structured as below: the second section will illustrate the mathematical model and analytical solutions; the third section will present the validation against existing experimental data and numerical models; the fourth section will perform a series of sensitive analyses regarding interface and substrate parameters.; the last section will summarize main conclusions draw in this article.

2 The Analytical Model and Solutions

2.1 The Analytical Model

A simplified mathematical model is presented in this section as sketched in Fig. 2a. It is assumed that the external force F is applied at the end of the unbonded reinforcement strip in a direction tangential to the strip axis. Materials and external forces are assumed to be uniform across the width of the reinforcement. As discussed previously, the model consists of three components: (i) a linear elastic FRP strip; (ii) a rigid and fixed masonry substrate; (iii) a zero-thickness interface that obeys a piecewise linear tangential stress-slip relationship dependent on the local normal stress (Fig. 2b), including three stages: the first linear elastic stage, the second linear descending softening stage, and the third constant residual tangential strength. It can be easily obtained by force analysis that, for the extrados case, the interface normal stress will be compressive thus a positive factor for friction, while the opposite for the intrados case. The mathematical expressions for the interface law are:

$$\begin{cases} \tau_1(s) = Ks & (0 < s \leq s_e) \\ \tau_2(s) = K_1 s + \tau^*_{\max}(1 - \frac{K_1}{K}) & (s_e < s \leq s_r) \\ \tau_3(s) = \tau_r & (s_r < s) \end{cases} \tag{1}$$

in which $\tau(s)$ is the tangential stress at the interface, a dependent variable of the slip of the FRP strip, s. Parameters K and K_1 indicate the slope of the elastic and softening stages, s_e is the maximum slip value of the elastic phase, s_u is the ultimate slip value for the flat case, s_e and s_r are the maximum slip value for the elastic and softening stages, respectively.

The maximum bond strength $\tau^*_{\max}$ and the interface residual strength τ_r depends on the interface normal stress σ_n:

$$\tau^*_{max} = \tau_{max} + \sigma_n tan\phi \tag{2}$$

$$\tau_r = \sigma_n \tan \phi_r \tag{3}$$

in which ϕ is the friction angle, and ϕ_r is the residual friction angle of the interface, τ_{max} is the maximum bond strength for the flat case. The values of these parameters usually can be inferred and presumed from experimental data.

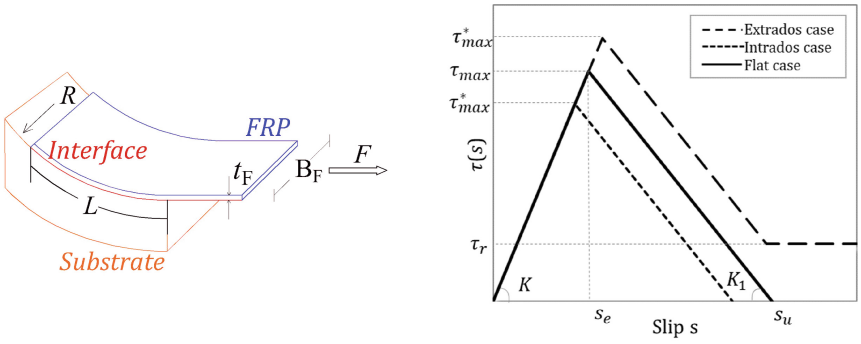

Fig. 2. The simplified mathematical model (a), and the interface law adopted (b).

2.2 Derivation of the ODE

For both extrados and intrados cases, an infinitesimal portion of the FRP strip is considered to gain the governing ODE. The longitudinal direction of the FRP strip is assumed to be x_1. The independent variable x ($0 \leq x \leq L$) defines the position of any point along the glued length L, and the abscissa $x = 0$ identifies the position of the free edge. The equilibrium of the infinitesimal portion of the reinforcement along the tangential direction x_1 can be written as follows for both the extrados and intrados cases:

$$t_F \frac{d\sigma_F}{dx} = \tau(s) \tag{4}$$

where σ_F is the tensile stress of the FRP strip along its longitudinal direction. The constitutive law for the elastic FRP material is:

$$\sigma_F = E_F \varepsilon_F \tag{5}$$

in which E_F is the elastic modulus, and ε_F is the normal strain of the FRP strip. With the assumption of the rigid substrate and subjected to no displacement, the interface slip value is equal to the elastic displacement of the FRP, i.e.:

$$\varepsilon_F = \frac{ds}{dx} \tag{6}$$

The governing ODE can be derived by substituting Eqs. (5) and (6) into Eqs. (4):

$$\frac{d^2s}{dx^2} = \frac{\tau(s, \sigma_n)}{E_F t_F} \tag{7}$$

To calculate the interface normal stress σ_n, write the equilibrium along the normal direction x_2:

$$\frac{d^2s}{dx^2} = \frac{\tau(s,\sigma_n)}{E_F t_F} \tag{8}$$

With the substitution of σ_n into the interface stress-slip law, Eq. (7) is a second-order non-linear differential equation with s and the dependent variable x. The following calculations will be given based on the extrados strengthening case, for the intrados case, it would be easy to replace the sign of the normal stress to gain the corresponding solutions.

2.3 The Closed-Form Solutions

To derive a closed-form solution for the previous ODE, it is necessary to assign a gradually increasing slip value s_0 at the free edge, so the following Initial Condition (Cauchy) problem can be written with the boundary conditions:

$$\begin{cases} \frac{d^2s}{dx^2} = \frac{\tau(s,\sigma_n)}{E_F t_F} \\ \left.\frac{ds}{dx}\right|_{x=0} = 0 \\ s(0) = s_0 \end{cases} \tag{9}$$

The slip value $s(x)$ will monotonically increase with x along the interface, considering three stages of the interface law, five possible situations will arise regarding the whole interface state: (i) only stage 1; (ii) stages 1 and 2; (iii) stages 1, 2 and 3; (iv) stages 2 and 3; (v) only stage 3. The following contents will present the closed-form solutions under the three different interface law stages, as well as the transformation points among different states that can be determined via the principle of continuity. The given slip value as the free end to trigger different situations can be reversibly determined by the known slip conditions for different interface states. Finally, the analytical procedure can be implemented into MATLAB to realize automatic calculation via any given material and geometric parameters. The calculation procedure will be terminated if a negative value appeared for the slope of the s-x relationship.

The First Stage. Let us assume that the first stage is active from the free edge up to x_e. A point with abscissa x_1 belonging to the elastic interface stage and its slip $s_1(x_1)$ can be obtained by solving the Cauchy problem Eq. (7) with $\tau(s,\sigma_n) = K_s$:

$$s_1(x_1) = \frac{s_0}{2}\left(e^{\gamma x_1} + e^{-\gamma x_1}\right) (0 \le x_1 \le x_e) \tag{10}$$

where, $\gamma = \sqrt{K/(E_F t_F)}$. If $x_e \leq L$, the value of x_e can be determined assuming that at x_e the tangential stress is equal to the maximum bond strength:

$$x_e = \frac{1}{\gamma} arcosh(X_a) = \frac{1}{\gamma} arcosh\left(\frac{\tau_{\max}}{\alpha_1 - \alpha_2}\right) \tag{11}$$

in which:

$$\begin{cases} x_a = \frac{\alpha_1}{\alpha_1 - \alpha_2} \\ \alpha_1 = E_F t_F s_0 \gamma^2 \\ \alpha_2 = E_F t_F s_0 \gamma \frac{\tan\phi}{R} \end{cases} \tag{12}$$

The Second Stage. The solutions at this stage can be obtained similarly:

$$s_2(x_2) = e^{\beta x_2}\left(C_1 \sin\sqrt{\alpha} x_2 + C_2 \cos\sqrt{\alpha} x_2\right) - \frac{1 - K_1/K}{K_1}\tau_{\max}(0 \leq x_2 \leq x_r) \tag{13}$$

in which:

$$\begin{cases} \alpha = -\left(\frac{K_1}{K} - 1\right)^2 \frac{\tan^2\phi}{4R^2} - \frac{K_1}{E_F t_F} \\ \beta = \frac{1}{2}\left(1 - \frac{K_1}{K}\right)\frac{\tan\phi}{R} \\ C_1 = \frac{1}{\sqrt{\alpha}}\left[\frac{s_0}{2}\left(e^{\gamma x_e} - e^{-\gamma x_e}\right) - C_2\beta\right] \\ C_2 = \frac{1 - K_1/K}{K_1}\tau_{\max} + \frac{s_0}{2}\left(e^{\gamma x_e} + e^{-\gamma x_e}\right) \end{cases} \tag{14}$$

The constants C_1 and C_2 can be determined via the continuous conditions at x_e:

$$\begin{cases} s_2(0) = s_1(x_e) \\ \frac{ds_2}{dx_2}|_{x_2=0} = \frac{ds_1}{dx_1}|_{x_1=x_e} \end{cases} \tag{15}$$

The Third Stage. To solve the Cauchy problem for the third stage, the following ODE with initial conditions is considered, where $x_2 = x_r$:

$$\begin{cases} \frac{d^2 s_3}{dx^2} = \frac{\tau_r}{E_F t_F} \\ s_3(0) = s_2(x_r) \\ \frac{ds_3}{dx_3}|_{x_3=0} = \frac{ds_2}{dx_2}|_{x_2=x_r} \end{cases} \tag{16}$$

3 Validations

3.1 Approaches for Validation

The experimental campaign conducted by Rotunno et al. [3] and the numerical model proposed by Milani et al. [12] were utilized for validation of the present model. The numerical model is based on the same experimental facts and adopts a similar mathematical model as in this present model. Only for a stable and robust calculation procedure, the numerical model assumes a smooth exponential function for the interface law. The

interface law also allows the incorporation of the interface normal stress, exhibiting an infinite ductility and an asymptotic residual strength in terms of the interface behavior.

The parameters needed in the present model are selected as the same in the numerical model proposed by Milani et al. As discussed in the literature [12], two approaches were developed to calibrate the parameters: the first one is a manual procedure adjusted by trial and error; the second more rigorous one is based on a least-square optimization. The comparisons of the gained values of parameters indicate that the two procedures provided similar results, leading to small differences from an engineering point of view. Thus, the first manual procedure was adopted out of convenience here.

The parameters involved are listed in Table 1. For the flat case, when assuming a large enough value for the substrate radius, the present model can be utilized as well. As an important parameter that controls the behavior of the residual strength stage, there is not enough experimental data to calibrate the parameter ϕ_r. In this study, it is assumed to be equal to the friction angle ϕ, due to the hypothesis that the friction angle defining the residual strength cannot be larger than that of the undamaged interface.

Table 1. Parameters adopted to validate the present model.

Label	R [mm]	E_F [MPa]	t_F [mm]	B_F [mm]	L [mm]	τ_{max} [N/mm^2]	s_e [mm]	s_u [mm]	ϕ [°]	ϕ_r [°]
CAE	1500	250000	0.165	100	382	1.37	0.093	0.324	35	35
CBE	3000	250000	0.165	100	354					
CAI	1500	250000	0.165	100	330					0
CBI	3000	250000	0.165	100	330					
Flat	10^8	250000	0.165	100	330				-	-

3.2 Results of the Analysis

Global Responses. As presented in Fig. 3, the results gained by the present analytical model (the black lines) are compared with the numerical results (the red line) and experimental data (the blue envelope). Thanks to the clear definition needed in the analytical solutions, the different stages situation of the interface can be indicated in the global curved via different line types. An increase after Stage 3 appeared on the interface is clearly expressed for the extrados strengthened cases (cases CAE and CBE), due to the non-zero residual friction strength. And this increase is more obvious under the higher substrate radius (Case CAE), due to a higher interface normal stress.

Compared with the numerical model, the results are quite similar in terms of the ultimate strength and slip values. The present model always exhibits slightly smaller strength values, due to the smaller shear stress values adopted in the assumed interface laws. And a major difference lies in the post-peak behavior, in our model, a snap-back phenomenon can be observed. The snap-back phenomenon indicates the unloading of the fiber strip due to the softening of the interface, which normally appears under a sufficiently long bond length. This phenomenon requires specific experimental set-ups to avoid the brittle sudden failure of the specimen after peak load is reached, the detail

and typical experimental results can be found in the literature [13]. The numerical model doesn't exhibit such behavior since, in that model, the ODE system is solved as a BVP (Boundary Value Problem), rather than an IVP (Initial Value Problem) in this analytical model. One boundary condition is the increasing known load applied at the loading edge of the FRP strip, naturally, the decrease of load and the snap-back phenomenon won't appear.

Compared with the experimental data, it can be concluded that the modeling curved is satisfactory in terms of the trend and ultimate load, however always yield an obviously smaller ultimate slip. This problem is identified in the numerical model. This can be attributed to the simplifications existing in the model which ignore the ductility of the strengthened system, for example, the possible internal slippage and damage of the FRP strip, the damage propagation inside the substrate, the interlocking effect due to the uneven surface around the mortar joints.

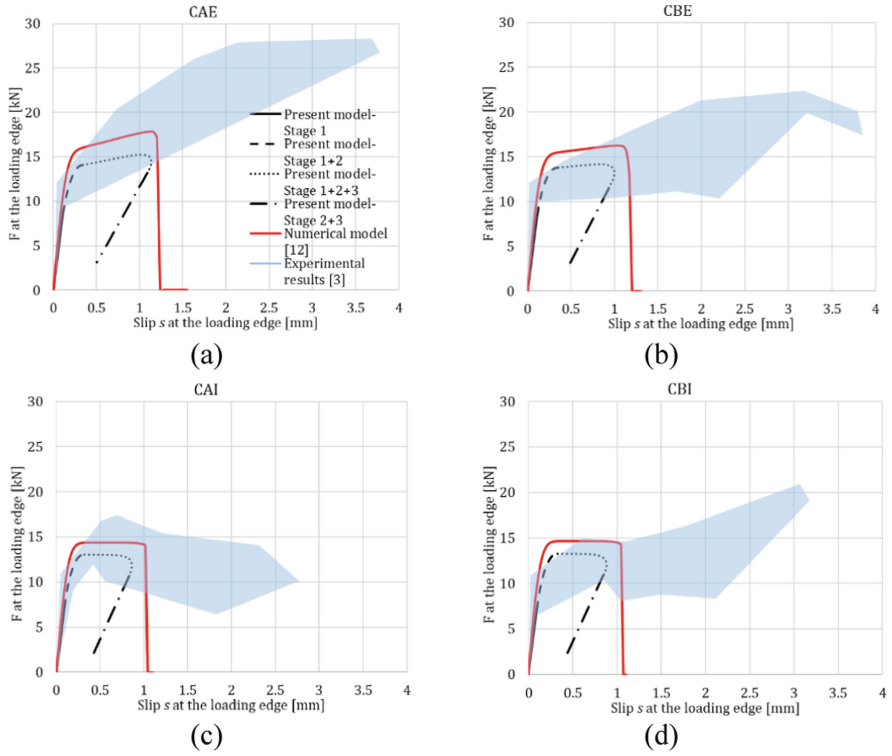

Fig. 3. Load-slip curves gained via the present model, numerical model [12], and shear tests [3] for case CAE (a), CBE (b), CAI (c), CBI (d).

Local Responses The current analytical procedure also allows determining the stress and displacement distributions along the interface. Take the case CAE as an example,

the results are presented in Fig. 4. The appearances of different interface stages are also available by the different colors and types of lines. The distinct divisions of the color (the interface stages) in the slip distribution (Fig. 4a) give a perfect verification of the correctness of the calculation. As can be normally observed in shear tests, the peak of the shear stress will gradually transfer from the loading edge to the free edge (Fig. 4b), and the stress level gradually declines towards the end of the loading procedure (Fig. 4c).

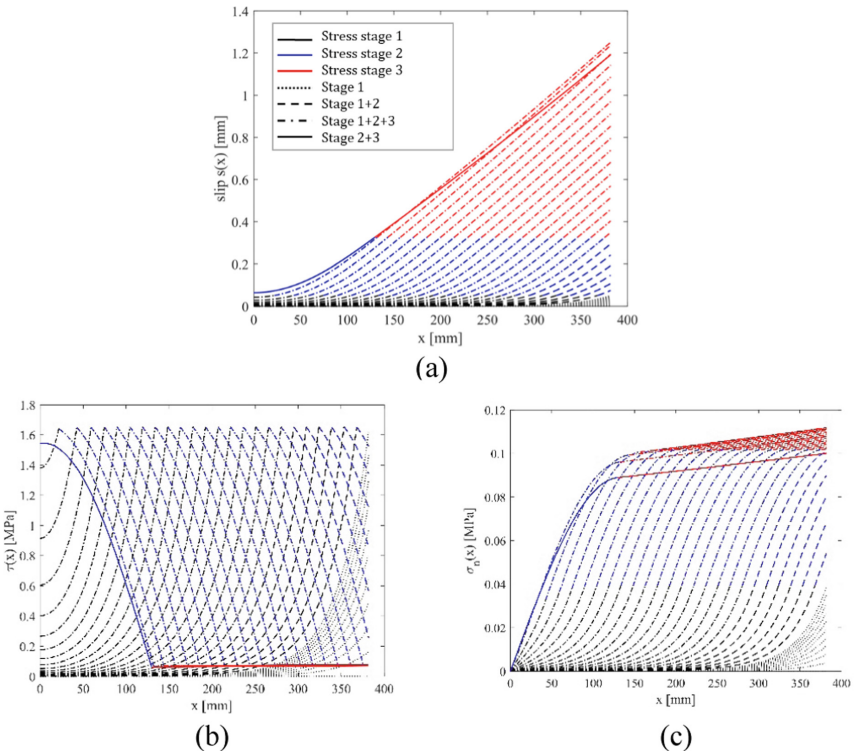

Fig. 4. Distributions of interface slip (a), shear stress (b), and normal stress (c) for case CAE.

4 Sensitive Analysis

For this present model dedicated to the curved substrate, it would be interesting to investigate the effect of substrate curvature on the relative parameter sensitivity. In the present model, the substrate curvature will affect the interface normal stress, and further influence the shear stress via the friction angles ϕ and ϕ_r by Mohr-Coulomb law. From common sense, when the curvature of the substrate is larger (closer to the flat case), the normal stress along the interface is smaller, which is consistent with the trend of the calculation results displayed in Fig. 5. And as the curvature of the substrate increases, the

bond strength will increase; the effect of friction angles on the intrados strengthening is smaller than that of the extrados strengthening, due to the smaller normal stress appearing intrados case.

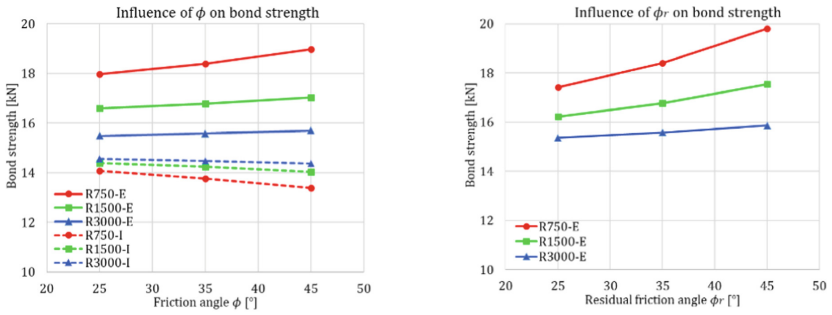

Fig. 5. Influences of ϕ (a) and ϕ_r (b) on bond strength for different substrate curvature radii.

5 Conclusions

In this article, a fast and stable analytical model was proposed to describe the bond behavior of FRP applied on curved substrates. The mathematical model was developed based on the shear test set-ups for FRP strengthened curved masonry prism. The non-linearities were all lumped at the interface, and a three-section line was adopted for the interface stress-slip law which will vary according to the interface normal stress. After comparing with the experimental load-slip curves, it can be considered that this present model can ideally reproduce the trend and ultimate strength. And the investigations on the influences of the parameters showed consistency with experimental observations as well. Moreover, compared to the numerical model solved as BVP, this model can reproduce the snap-back phenomenon.

However, both the present model and the numerical model exhibit a smaller ultimate strength due to the simplifications that ignored the ductility of the strengthened system. Further studies may take into account the deformation and damage of the substrate, or change the mathematical formula for describing the post-peak interface behavior, to improve the ductility of the model.

Acknowledgments. Yu Yuan would like to acknowledge the financial support provided by the Chinese Scholarship Council (CSC) for performing her Ph.D. program at the Technical University of Milan, Italy.

References

1. Valluzzi, M.R., Modena, C., de Felice, G.: Current practice and open issues in strengthening historical buildings with composites. Mater. Struct. **47**(12), 1971–1985 (2014). https://doi.org/10.1617/s11527-014-0359-7
2. Vaculik, J., Visintin, P., Burton, N.G., Griffith, M.C., Seracino, R.: State-of-the-art review and future research directions for FRP-to-masonry bond research: Test methods and techniques for extraction of bond-slip behaviour. Constr. Build. Mater. **183**, 325–345 (2018). https://doi.org/10.1016/j.conbuildmat.2018.06.103
3. Rotunno, T., Fagone, M., Bertolesi, E., Grande, E., Milani, G.: Single lap shear tests of masonry curved pillars externally strengthened by CFRP strips. Compos. Struct. **200**, 434–448 (2018). https://doi.org/10.1016/j.compstruct.2018.05.097
4. Rotunno, T., Fagone, M., Bertolesi, E., Grande, E., Milani, G.: Curved masonry pillars reinforced with anchored CFRP sheets: an experimental analysis. Compos. B Eng. 174, 107008 (2019).https://doi.org/10.1016/j.compositesb.2019.107008
5. Valluzzi, M.R., Valdemarca, M., Modena, C.: Behavior of brick masonry vaults strengthened by FRP laminates. J. Compos. Constr. **5**(3), 163–169 (2001). https://doi.org/10.1061/(ASCE)1090-0268(2001)5:3(163)
6. Oliveira, D.V., Basilio, I., Lourenço, P.B.: Experimental behavior of FRP strengthened masonry arches. (2010). https://doi.org/10.1061/(ASCE)CC.1943-5614.0000086
7. Carozzi, F.G., Poggi, C., Bertolesi, E., Milani, G.: Ancient masonry arches and vaults strengthened with TRM, SRG and FRP composites: experimental evaluation. Compos. Struct. **187**, 466–480 (2018). https://doi.org/10.1016/j.compstruct.2017.12.075
8. Carloni, C., Focacci, F.: FRP-masonry interfacial debonding: an energy balance approach to determine the influence of the mortar joints. Eur. J. Mech. A. Solids **55**, 122–133 (2016). https://doi.org/10.1016/j.euromechsol.2015.08.003
9. Caggiano, A., Martinelli, E., Faella, C.: A fully-analytical approach for modelling the response of FRP plates bonded to a brittle substrate. Int. J. Solids Struct. **49**(17), 2291–2300 (2012). https://doi.org/10.1016/j.ijsolstr.2012.04.029
10. Grande, E., Milani, G.: Modeling of FRP-strengthened curved masonry specimens and proposal of a simple design formula. Compos. Struct. **158**, 281–290 (2016). https://doi.org/10.1016/j.compstruct.2016.09.017
11. Fedele, R., Milani, G.: A numerical insight into the response of masonry reinforced by FRP strips. the case of perfect adhesion. Compos. Struct. **92**(10), 2345–2357 (2010). https://doi.org/10.1016/j.compstruct.2010.03.014
12. Milani, G., Fagone, M., Rotunno, T., Grande, E., Bertolesi, E.: Development of an interface numerical model for C-FRPs applied on flat and curved masonry pillars. Compos. Struct. **241**(7), 112074 (2020b). https://doi.org/10.1016/j.compstruct.2020.112074
13. Carrara, P., Ferretti, D., Freddi, F.: Debonding behavior of ancient masonry elements strengthened with CFRP sheets. Compos. B Eng. **45**(1), 800–810 (2013). https://doi.org/10.1016/j.compositesb.2012.04.029